Electronic band structure of metallic calcium measured by electron momentum spectroscopy

2000 J. Phys.: Condens. Matter 12 9407

(http://iopscience.iop.org/0953-8984/12/45/304)

J. Phys.: Condens. Matter **12** (2000) 9407–9423. Printed in the UK PII: S0953-8984(00)15756-X

Electronic band structure of metallic calcium measured by electron momentum spectroscopy

V A Sashin†, M A Bolorizadeh†§, A S Kheifets‡ and M J Ford†‖

† School of Chemistry, Physics and Earth Science, Flinders University of South Australia, GPO Box 2100, Adelaide, SA 5001, Australia

‡Research School of Physical Sciences and Engineering, Institute of Advanced Studies, ANU, Canberra, ACT 0200, Australia

E-mail: michael.ford@flinders.edu.au

Received 24 July 2000, in final form 21 September 2000

Abstract. We have measured the bulk energy–momentum resolved conduction band structure of metallic calcium using electron momentum spectroscopy (EMS). From the EMS data we have extracted the band dispersion, occupied bandwidth and density of states. The experimental results are compared with band structure calculations performed within the linear muffin-tin orbital (LMTO) approximation. The free-electron parabola expected for the dispersion relation in a metallic solid is clearly reproduced in the experimental data and is in good agreement with our calculation. A background produced by multiple-scattering events within the target is also evident in the EMS results. In order to make a quantitative comparison, we have included the effects of multiple scattering in the calculation using a Monte Carlo (MC) simulation. The results of this procedure reproduce the measured conduction band features and background intensity very well. The occupied bandwidth is measured to be 3.3 ± 0.2 eV, and agrees with previous measurements and the value predicted by our LMTO calculation when the MC simulation is included. However, the experiment indicates that the band dispersion curve is narrower in momentum by as much as 0.1 au compared with the theory. We have also made measurements of the energies of the 3s and 3p core levels in metallic calcium, and obtained values of 45.0 ± 0.4 eV and 25.6 ± 0.2 eV respectively. These results are in good agreement with previous experiments.

1. Introduction

The alkaline-earth elements, with closed-shell ns^2 electronic configurations, form so-called semi-metals in the solid phase that derive their metallic properties from band overlap. The band structure of these solids is expected to be close to the simple, free-electron-like parabola. A number of theoretical calculations have been performed which support this assertion. Experimental results, on the other hand, are more limited and generally do not reveal the full band dispersions. In the case of Ca, the electronic structure is complicated by the fact that the 3d orbitals, which are essentially empty in the free atom, lie in close proximity to the valence 4s orbitals. Hybridization can then give rise to appreciable 3d character in the conduction band of metallic Ca at the Fermi level. Indeed, band structure calculations indicate that 0.5 3d electrons become admixed with the predominantly s-like conduction band due to this s–p/d hybridization [1]. The influence of d and p bands upon the properties of metallic Ca has been demonstrated in, for example, the Fermi surface topology [2], and metal–semimetal–metal electronic transition [3] that occurs under increasing pressure. The latter have been explained in calculations including d orbitals by an avoided s–p band crossing [4].

§ Permanent address: Physics Department, Shahid Bahonar University, Kerman, Iran.
‖ Corresponding author.

0953-8984/00/459407+17$30.00

The first band structure calculations for calcium were reported more than 60 years ago by Manning and Krutter using the cellular method [5]. Since that time, the bulk properties of calcium and the other alkaline earth metals have been the subject of extensive theoretical investigation. These studies have employed a range of techniques, such as cellular [6], pseudopotential [7], orthogonalized plane wave [8], density functional theory (DFT) within the local density approximation (LDA) [9] and others. By contrast, experimental reports of the electronic structure of calcium, and indeed the alkaline earths in general, are much scarcer. The core-level electronic structure has been studied using x-ray photoelectron [10, 11] (XPS) and Auger electron spectroscopy [12]. These measurements provide binding energies of the core-levels and demonstrate the effect of d states on the satellite emission spectrum. Resonant enhancement of the valence-band photoemission spectrum measured by Barth *et al* [13] also demonstrates the importance of many-body effects in metallic Ca. Surface and bulk conduction band densities of states and bandwidths have been determined by Ley *et al* [14] using surface enhanced XPS, by Kingston [15] from emission spectra following electron bombardment and by Finkelshteyn and Nemnonov [16] using soft x-ray measurements. However, some discrepancies exist in bandwidth estimates obtained by these methods, and values calculated in previous theoretical studies. To our knowledge there have been no measurements of the full energy and momentum resolved band structure of Ca reported to date.

In this paper we report the electronic structure of calcium measured by electron momentum spectroscopy (EMS). This technique has already proved its ability to provide detailed electronic structure information for atoms and molecules [17], and more recently has been applied to solid-state targets [18–21]. EMS provides information which is complementary to the more familiar technique of angle resolved photoemission (ARPES). It can map the band dispersion together with band occupation in a very direct way, and unlike ARPES is equally applicable to crystalline, polycrystalline or amorphous structures. We have also calculated the band structure using the full-potential linear muffin-tin orbital (FP-LMTO) method. In order to make a detailed comparison between experiment and theory, a Monte Carlo simulation of multiple scattering effects has been included in the theoretical study. This work aims to provide a complete measurement of the band structure of metallic Ca and to shed further light on discrepancies observed in our previous comparisons of EMS measurements and LMTO calculations for Mg [20] and Si [21].

2. Experimental techniques

2.1. (e, 2e) spectrometer

The spectrometer used in the current work has already been described in detail in the literature [22], here we limit ourselves to a short outline of some pertinent points relating to its operation.

The momentum and energy probability distribution of electrons in an atomic, molecular or solid target can be mapped via the so-called (e, 2e) reaction [17, 23]. This process refers to electron impact ionization events where a high energy incident electron transfers considerable momentum to the electron ejected from the target. Under these conditions the (e, 2e) collision can be regarded as a 'billiard-ball'-like collision between the incident and target electron, the core of the target being a spectator which provides the binding energy of the struck electron. Spectroscopy of the target electronic structure is then performed by specifying completely the kinematics of the collision. The energy and momentum of the incident electron beam is well defined and the energies and momenta of the two outgoing electrons are measured under the so-called Bethe ridge condition [24]. Simply put, the Bethe ridge corresponds to the angle one would expect the incident electron to be scattered through in a 'billiard-ball'-like collision with

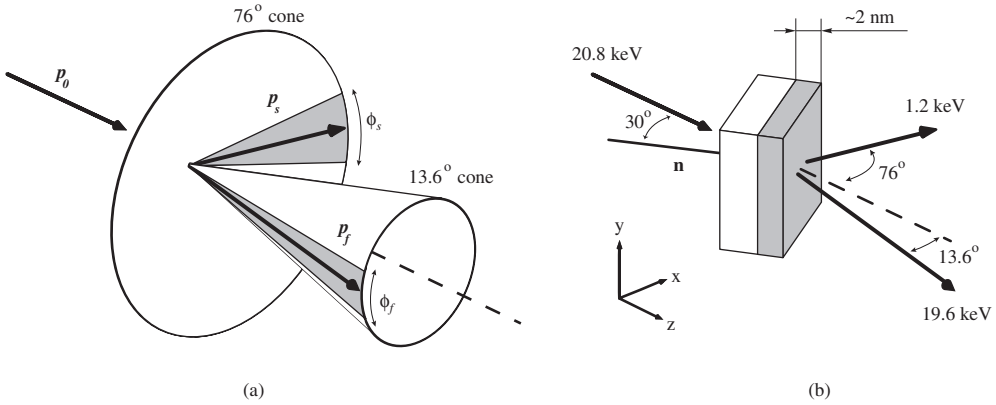

Figure 1. Schematic diagram of (a) the scattering geometry, and (b) target orientation with respect to incident and outgoing electrons. The shaded area in (a) indicates the angular acceptance of the analysers and that in (b) represents the portion of the target that contributes most to the measured energy–momentum density.

the target electron. The binding energy ε and momentum $\boldsymbol{q}$ of the target electron immediately before ionization can then be determined by the conversation of energy and momentum:

$$\varepsilon = E_0 - E_s - E_f \qquad \boldsymbol{q} = \boldsymbol{p}_s + \boldsymbol{p}_f - \boldsymbol{p}_0$$

where $(E_0, \boldsymbol{p}_0)$ denotes the energy and momentum of the incident electron respectively; $(E_s, \boldsymbol{p}_s)$ and $(E_f, \boldsymbol{p}_f)$ are the same parameters for two outgoing electrons. An (e, 2e) cross-section is measured as a function of the energies and momenta of the outgoing electrons. This cross-section is proportional to the probability of the target electron having a particular binding energy and momentum multiplied by the half-off-shell Mott electron–electron scattering cross-section. The Mott cross-section can be considered essentially constant over a suitable range of detection energies and angles [17, 23]. The overall (e, 2e) cross-section is therefore proportional to the absolute square of the target electron wavefunction in momentum space, hence the name electron momentum spectroscopy.

The scattering geometry of our (e, 2e) spectrometer is presented in figure 1(a). The spectrometer operates in transmission mode with the outgoing electrons detected on the opposite side of the target from the incident beam. As can be seen from the picture it exploits strongly asymmetric non-coplanar kinematics. The incident and two detected electron energies are nominally 20.8, 19.6 and 1.2 keV respectively. The outgoing electrons are accepted into the electrostatic energy analysers at polar angles of 13.6 and 76° relative to the direction of the incident beam. The entrance aperture of the fast electron (19.6 keV) analyser accepts electrons over ±6° azimuthal angles relative to the x–z horizontal plane, and similarly the acceptance of the slow electron (1.2 keV) analyser is ±10°. The overall momentum detection range with the above parameters is ±2.5 au. The scattering geometry means that (e, 2e) events are accepted for target electrons that originally had their momenta directed along the y-axis in figure 1. In the case of single crystal targets this feature allows us to measure electronic structure along a specific crystal direction [21]. The overall energy and momentum resolutions of the spectrometer are 1 eV and 0.1 au respectively.

The electron energy analysers operate in a parallel detection mode; electrons leaving the collision centre over a range of energies and azimuthal angles are accepted. Position sensitive microchannel plates in combination with a resistive anode encoder in each analyser allow us to determine the energy and momentum coordinates of each detected electron. Fast timing pulses

are also derived from the microchannel plates that are used to measure the time difference of a pair of electrons, one arriving at each analyser. Electrons from the same ionization event will be highly correlated in time, and the coincidence, or time spectrum allows us to discriminate these electrons from random pairs and from the background due to other scattering events.

The most important attribute of the spectrometer is its near-surface sensitivity. The relatively small escape depth of the 1.2 keV electron means that the electronic structure information comes predominantly from the outermost 2 nm of the target facing the analysers. This area of the target is shaded in figure 1(b). Ionization events occurring deeper within the target contribute only to the background in the (e, 2e) intensity. This near-surface sensitivity has its negative and positive sides. The negative side is that one needs to prepare extremely thin targets in order to avoid the signal being dominated by multiple scattering [21, 25]. On the positive side, targets can be prepared by evaporation onto a thin substrate without the substrate contributing to the results. The latter property has been exploited in the current work and our previous measurements on Mg/MgO targets [20].

2.2. Sample preparation

Calcium targets are prepared *in situ* using a simple resistively heated evaporator. The metal (99% purity) is evaporated onto 5 nm thick amorphous carbon films. These are perfect substrates for our sample preparation as they are extremely durable, inert and of relatively low atomic number. Before Ca deposition the a-C films are annealed to remove all impurities from the surface. A number of targets were prepared with a range of Ca coverages from 1 to 10 nm, a Ca layer of 5 nm was found to produce an optimal (e, 2e) signal. Deposition rates were monitored using a quartz crystal microbalance. Background pressure of the evaporation chamber is maintained at a level of 10^{-10} Torr and deteriorates by about one or two orders of magnitude during evaporation, depending on the previous degassing history of the calcium sample. The structural nature of the deposited films is expected to be polycrystalline.

A differential Auger spectrum taken immediately after Ca deposition is presented in figure 2(a). Only Ca Auger lines are present implying that the surface is clean. The $M_{2,3}VV$ line at about 20 eV, four $L_{2,3}M_{2,3}M_{2,3}$ transitions ranging from 292 eV to 303 eV and the $L_{2,3}M_{2,3}V$ line at about 325 eV are the signature of pure elemental calcium. An important question arises as to whether the Ca overlayer completely covers the a-C substrate or forms 3D islands at the optimal coverage. The absence of a carbon signal in the Auger spectrum suggests the coverage is complete, although the small bump around 260 eV might be ascribed to the C KVV transition. However, it can also belong to the Ca $L_{2,3}M_1M_1$ line, or be a 35 eV energy loss structure associated with the intense Ca $L_{2,3}M_{2,3}M_{2,3}$ line as suggested by Vayrynen *et al* [12]. In any case, the carbon presence at the surface is minimal, if it exists at all, and, furthermore, no signal is observable from the substrate in the EMS data

Elemental calcium readily reacts with the residual background gases present in the spectrometer vacuum chamber. Even though UHV conditions of about 5×10^{-10} Torr are maintained, approximately 2 days of data collection are required in total to achieve good statistics in the EMS data: reaction of the Ca sample with residual gases is clearly an important consideration. This problem of chemical reactivity is illustrated in figure 2(b). The Auger electron spectrum shown was measured after exposing an initially clean Ca sample to the spectrometer base pressure for 22 hours. The oxygen KVV line at about 510 eV and nitrogen KVV line at 381 eV have appeared, the Ca $M_{2,3}VV$ line has nearly vanished together with drastic changes in the shape of the other calcium lines. From figure 2(b) it is clear that the Ca sample will undergo a significant reaction with residual oxygen, and to a lesser extent nitrogen, during the time required to collect the EMS data. To overcome this problem we have

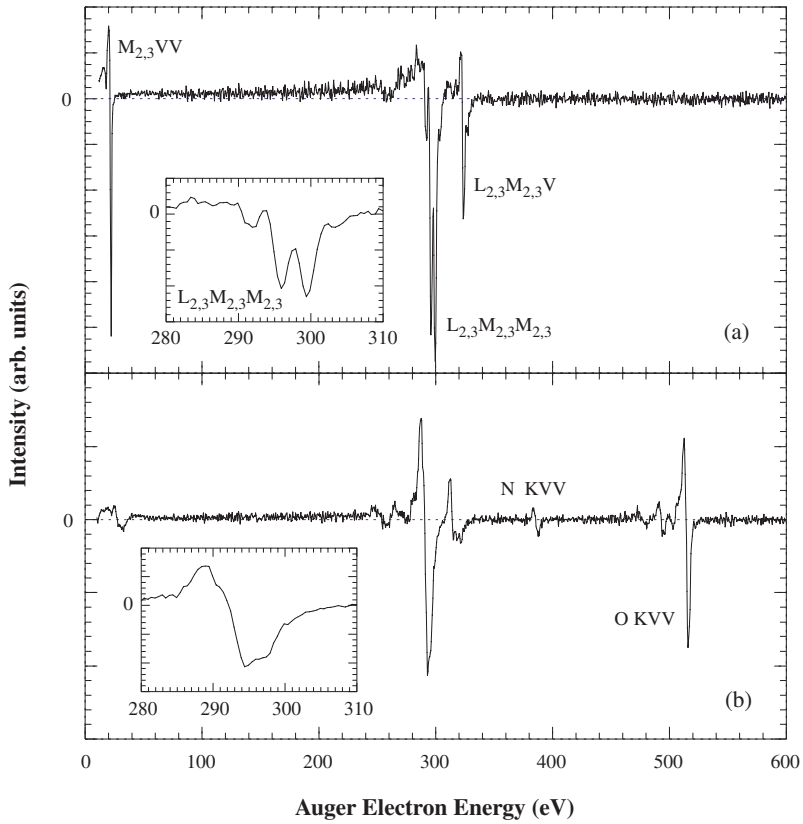

Figure 2. Differential Auger electron spectrum of the calcium target, (a) immediately after deposition, and (b) after 22 hours under UHV conditions in the spectrometer. Insets show magnified views of the Ca $L_{2,3}M_{2,3}M_{2,3}$ transition.

performed EMS measurements on a number of Ca samples and added together only the initial portion of data collected for each sample. A similar approach was necessary in our recent measurements on Mg [20].

We have attempted to quantify the rate at which the calcium sample oxidizes under the UHV conditions of our spectrometer by measuring the electron energy loss spectra for 19.6 keV electrons in a standard 5 nm thick Ca target every four hours. A series of these spectra taken over a 24 hour period is presented in figure 3. Four energy loss features are clearly visible in the spectrum measured one hour after calcium deposition. The first feature at about 22 eV is due to a bulk plasmon energy loss in the a-C substrate. There is a noticeable deviation of 3 eV in the position of this peak compared with the value reported by Egerton [26] that can be attributed to a density effect (see, for example [27]). The second peak at about 8.5 eV is due to the bulk plasmon in Ca. The last two peaks at about 3.5 eV and 35 eV are due to interband transitions in Ca. The a-C peak and the 35 eV peak from Ca are stable in time, whereas the intensity of the other two peaks decreases with increasing exposure due to oxidation of the Ca.

At an electron energy of 19.6 keV the mean free path for bulk plasmon excitation in Ca, calculated from an expression derived by Quinn [28], is about 60 nm, a value which is much larger than the initial thickness (5 nm) of the deposited Ca layer. Hence, the dependence of the probability of exciting one bulk plasmon as a function of sample thickness can be approximated

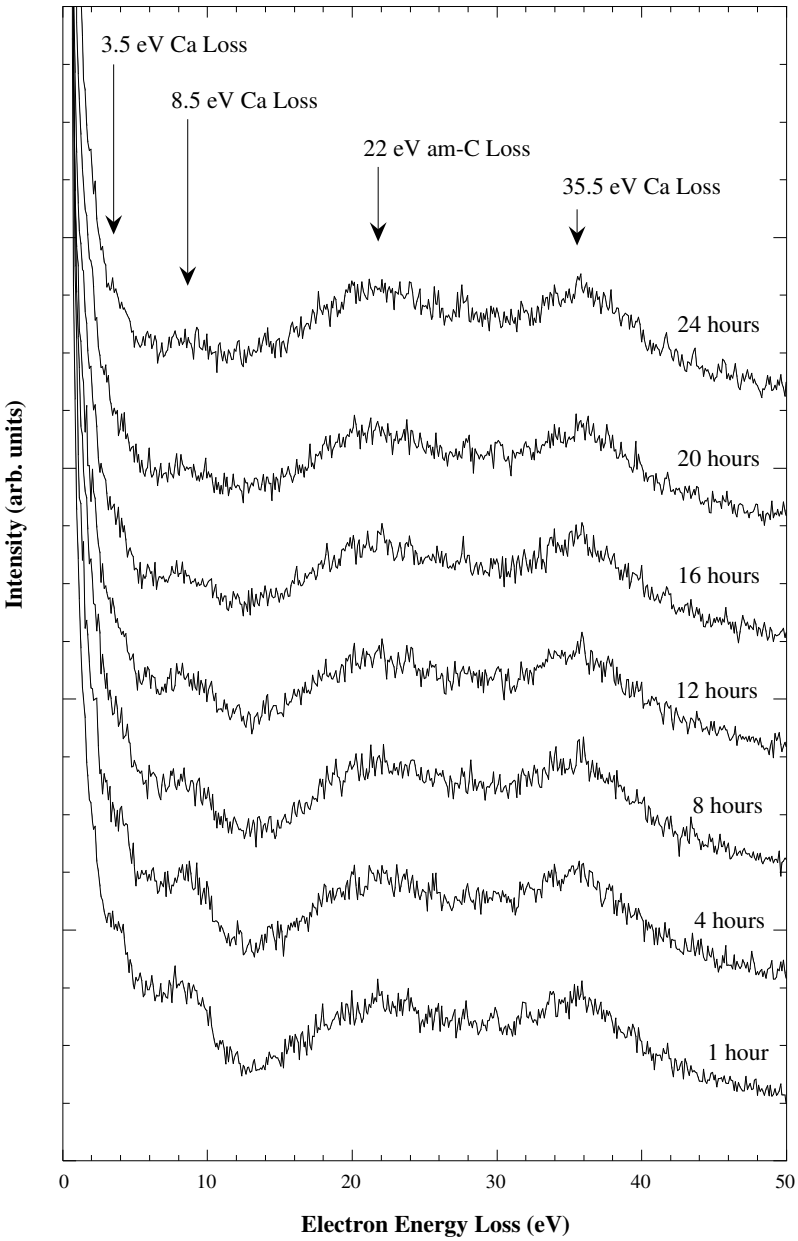

Figure 3. Evolution of the electron energy loss spectrum for a 5 nm Ca film deposited onto a 5 nm a-C substrate over a period of 24 hours under UHV conditions. Incident electron energy is nominally 19.6 keV and electrons are detected at a 13.6° scattering angle. The vertical arrows indicate characteristic energy losses in the two layers.

by a linear function, and the intensity of the corresponding energy loss feature is a good measure of the thickness of the unoxidized Ca layer. The intensity of the 8.5 eV bulk plasmon peak as a function of time is shown in figure 4. There are two distinctive time intervals in this graph. During the first 15 hours the intensity falls continuously, corresponding to oxidation

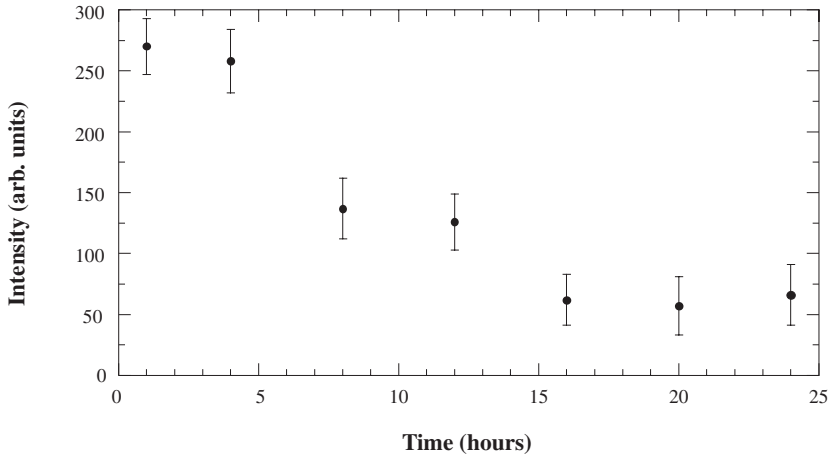

Figure 4. Intensity of the 8.5 eV bulk plasmon in the calcium film as a function of time, under UHV conditions.

of the Ca layer. After this period, the intensity remains constant implying that oxidation has progressed through the entire Ca film. The slope of this graph during the first period gives an estimated oxidation rate of about 0.3 nm per hour. From this value, the 2 nm layer probed by the EMS measurement will be completely oxidized after 7 hours. In the present data therefore, we retain only the first two hours of collection, with data from four samples added together to give sufficient statistics in the final results.

3. LMTO calculation and Monte Carlo simulation

The band structure and the electron momentum density were calculated using the FP-LMTO method as described in Kheifets *et al* [29]. The lattice parameter, according to Wyckoff [30] was 10.537 au. The local density approximation was used with the Janak–Moruzzi–Williams parametrization to the exchange–correlation functional. The Fermi energy E_F and energy of the K_1 symmetry point (both relative to the Γ_1 point) are shown in table 1.

Our calculation is similar to the LMTO calculation of Jan and Skriver [2], who used an atomic sphere approximation to the LMTO. They found that an empirical shift of the positions of the p and d bands relative to the s band should be introduced to reproduce correctly the Fermi surface topology. With this shift their results were found in agreement with an early phenomenological calculation employing the Gaspar potential [31]. A wrong Fermi surface topology predicted by an *ab initio* LMTO calculation is, most likely, due to some correlation effects which are not taken into account by the local density approximation.

The calculated band dispersions and electron momentum densities in several high-symmetry directions are shown in figure 5. We note the Fermi level intersects the bands both in ΓK and ΓL directions. In the *ab initio* LMTO calculation of Jan and Skriver [2] the Fermi break in ΓK does not exist.

A direct comparison of the experimental EMS results with the LMTO calculation allows one to draw only qualitative conclusions. For a more quantitative analysis the multiple scattering background must be accounted for. This background arises in the experimental data due to electrons from an (e, 2e) event undergoing additional small angle elastic scattering and/or inelastic scattering (plasmon excitation or valence electron excitation).

Table 1. Energy band parameters in eV.

	Local density [2]	Local density adjusted [2]	Gaspar potential [31]	Present
E_F	4.030	5.143	4.830	3.96
$E(\mathrm{K}_1)$	4.022	5.457	4.762	3.99

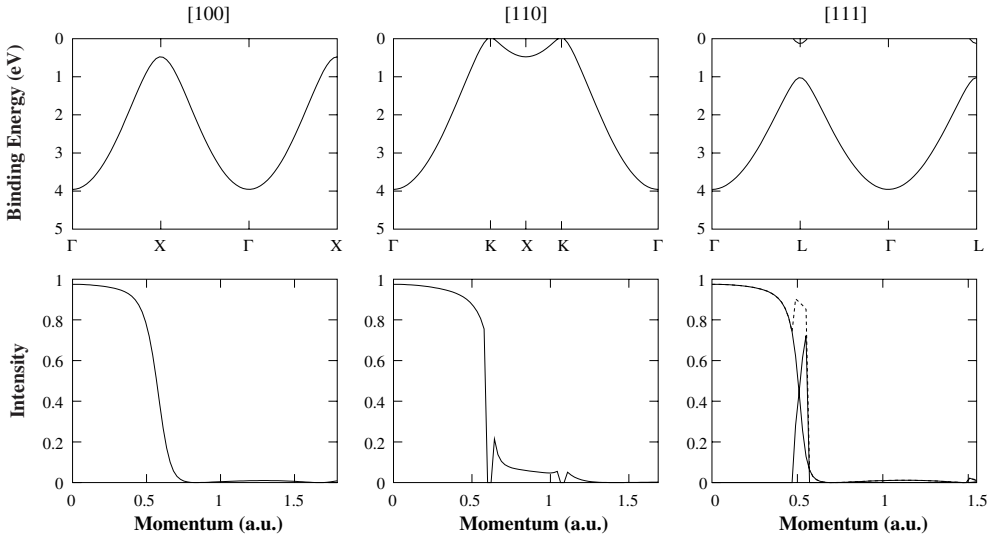

Figure 5. Band dispersions (top row) and electron momentum densities for Ca calculated within the LMTO approximation along several high symmetry directions.

There are two potential approaches to a full analysis of the data. The first would lie in developing a procedure for deconvoluting the experimental data to get a 'pure' EMS spectrum free from the multiple scattering background. This approach could be fruitful if the deconvolution function is well established and the level of the background is low compared to the clean (e, 2e) signal. Even for extremely thin targets used in our EMS experiments (i.e. less than 10 nm thick) the multiple scattering background is still large, particularly in the case of metals and semiconductors where plasmon excitation probabilities are large. Extracting a 'pure' EMS spectrum is a very problematic task. This approach has been used with limited success in previous (e, 2e) measurements [32]. The second approach is based on simulating multiple scattering in the theoretical spectrum using, for example, a Monte Carlo procedure. This method can, in practice, be implemented more easily than the former to give reasonable results. It must be noted, however, that both approaches relay upon an adequate description of the interaction of electrons with the solid target.

A FORTRAN Monte Carlo (MC) code was written a few years ago and enables us to simulate multiple scattering in elemental metals and semiconductors [33]. Despite the fact that this code uses a relatively simple description of the experimental geometry and the nature of the background, it has been applied with reasonable success to the interpretation of EMS data (see, for example [19, 20, 34]). However, the intensity of the simulated background is noticeably smaller than the experimental result. Recently, we have developed the MC simulation code further to include some specific features of electron energy loss processes in calcium and improve some other parameters of the program.

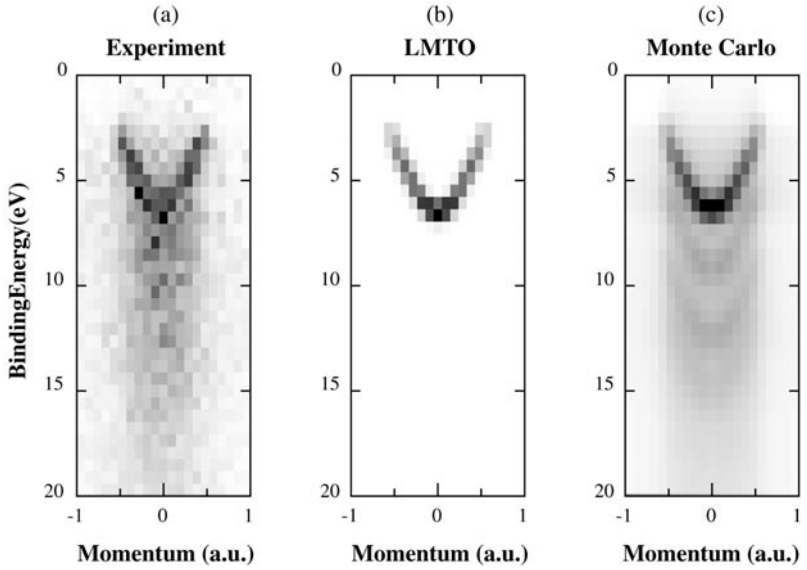

Figure 6. Energy and momentum resolved densities of metallic Ca, (a) measured by EMS, (b) calculated within the LMTO approximation, spherically averaged and convoluted with experimental energy and momentum resolutions, (c) simulated by the Monte Carlo procedure using the LMTO calculation as input. The LMTO and MC results have been shifted by 2.4 eV to match the experimental binding energy referenced to the vacuum level. Intensity is on a linear grey scale with darker colour representing higher intensity.

4. Results and discussion

4.1. Conduction band

A grey-scale plot of the experimental energy and momentum resolved density in the conduction band of calcium is presented in figure 6(a). This figure represents the band structure in the extended zone scheme and since the sample is expected to be polycrystalline is a spherical average over all crystal directions. The figure is plotted in terms of electron momentum rather than the more conventional symmetry points because the EMS experiment measures real momentum and not crystal momentum. Binding energies are relative to the vacuum level. The data have been binned into 0.6 eV and 0.1 au energy and momentum intervals respectively. These parameters are chosen as a compromise between achieving good statistics and still retaining sufficient energy and momentum resolution. Darker colour corresponds to higher intensity within the bands, with the intensity related to the ground state occupation or density. A free-electron-like parabola characteristic of a metallic solid is clearly visible. It is symmetric about zero momentum and disperses in binding energy from approximately 3 eV to 6.5 eV. The spread in momentum is about 0.5 au.

A significant background intensity is present due to multiple scattering of the incoming and/or outgoing electrons comprising (e, 2e) events. Small angle elastic scattering changes the momentum of the electron and results mainly in a smearing of the (e, 2e) intensity along the momentum axis. Inelastic scattering due to plasmon excitation or valence electron excitation changes the energy of the electron and shifts intensity along the energy axis. In the case of plasmon excitation this energy loss has a fixed value, and if the excitation probability is relatively high, replicas or ghosts of the main conduction band feature are observed shifted to

higher binding energies by multiples of the plasmon energy. In figure 6(a) four areas of higher intensity are observable at about 2, 4, 6 and 9 eV below the conduction band. Though the intensity of these features is at the level of statistical fluctuations, this series of energy values reproduces very well the characteristic bulk energy losses in metallic calcium of 4.1 and 8.7 eV and their surface counterparts of 1.8 and 6.8 eV [35]. Two of these features are also present in our energy loss spectrum shown in figure 3 for 'clean' Ca, i.e. after 1 hour exposure. These are the peak at 8.5 eV attributable to the Ca bulk plasmon and one at 3.5 eV which could be derived from interband transitions in Ca [36]. Surface plasmon loss features, however, are not visible.

Figure 6(b) shows the energy and momentum resolved density calculated using the LMTO method. This is a spherical average over the irreducible wedge of the Brillouin zone to account for the polycrystalline structure of the Ca sample and has additionally been convoluted with two Gaussians corresponding to the experimental energy and momentum resolutions. The data have been binned in the same way as figure 6(a) and binding energies are also relative to the vacuum level. A single free-electron-like parabola is evident. Using this LMTO calculation as input into the Monte Carlo simulation we produce the plot shown in figure 6(c). An overall background due to multiple scattering is clearly visible together with replicas of the conduction band parabola at higher binding energies. At least three replicas can be observed corresponding to excitation of the 2 and 6 eV surface and 9 eV bulk plasmons in Ca. There is good agreement between the LMTO calculation plus MC simulation in figure 6(c) and the experimental result in figure 6(a).

In order to make quantitative comparisons of our results we have taken slices along the energy axis in figure 6 integrated over 0.1 au momentum intervals; the resulting binding energy plots are presented in figure 7. Since the band structure is symmetric around zero momentum we have summed positive and negative momentum values to improve the statistics. Band intensities for all three sets of data are normalized at 0 au momentum. There is excellent agreement between the intensities of the main conduction band peak from the experiment, LMTO calculation and LMTO plus MC simulation. The only variance occurs at 0.6 au momentum where the MC simulation predicts a slightly higher value, although within this interval the MC background intensity is also higher than experiment across most of the binding energy spectrum. Similar behaviour of the background is observed at 0.5 au momentum. Overall the MC results simulate the experimental background intensity and structure very well; this is in contrast to the original MC code, which produced intensities around 50% smaller than the experiment (see for example [20]).

The width of the conduction band peaks is determined by a combination of the spectrometer resolution, small inelastic energy losses and physical line broadening such as life-time effects [19, 37]. Even with inclusion of the spectrometer resolution, the LMTO calculation produces peak widths which are considerably narrower than experiment. With the addition of inelastic energy loss processes the MC simulation gives good agreement, except at 0 au momentum. This discrepancy may be evidence of life-time broadening effects being important.

We have also sliced the data in figure 6 along the momentum axis integrated over 0.5 eV intervals to produce the momentum profiles shown in figure 8. All the intensities are normalized in the energy interval centred at 6.37 eV, which corresponds to the bottom of the experimental conduction band. As can be seen from the figure the Monte Carlo curves reproduce the experimental data reasonably well, giving comparable widths for momentum peaks. However, there is a difference in intensity for energy intervals centred at 2.87 eV to 4.37 eV and for 7.37 and 7.87 eV. The last two energies are below the bottom of the conduction band and MC shows much less intensity at momentum values less than 0.3 au.

The most significant discrepancy between experiment and theory occurs for the dispersion of the conduction band, as is evident by comparing measured and predicted peak positions both

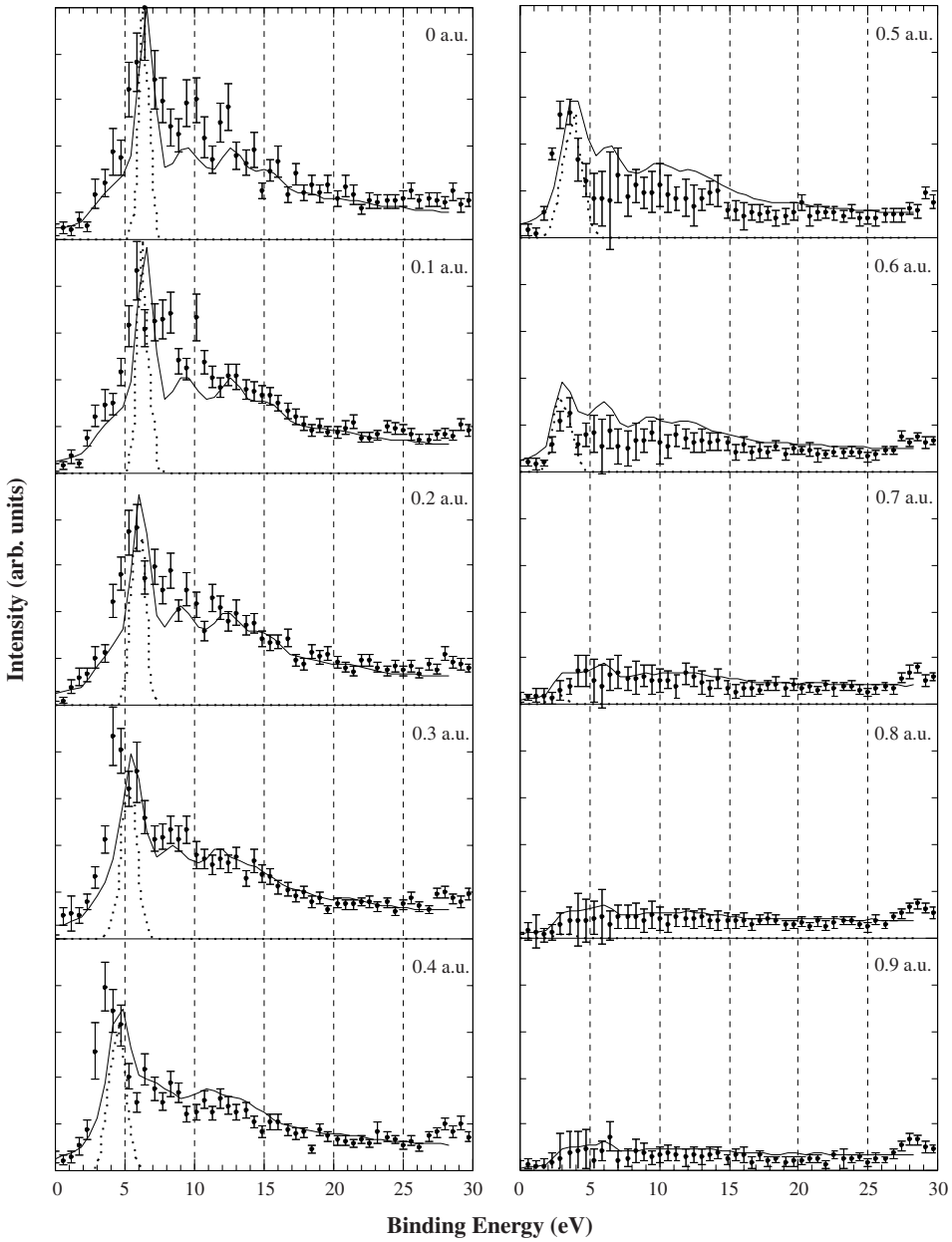

Figure 7. Binding energy spectra for Ca integrated over 0.1 au momentum intervals from the experiment (points with error bars), the Monte Carlo (MC) simulation (solid lines), and the LMTO calculation (dashed lines). The three data sets have been normalized in the momentum interval $0 < q < 0.1$ au. The LMTO and MC curves have been shifted by 2.4 eV to match the experimental binding energy referenced to the vacuum level.

for the binding energy spectra (figure 7) and momentum profiles (figure 8). To examine this further we have extracted dispersion curves from all three sets of data (experiment, MC and theory) using a least squares fit to determine accurate peak positions. The binding energy spectra in figure 7 were fitted with a Gaussian function to approximate the conduction band

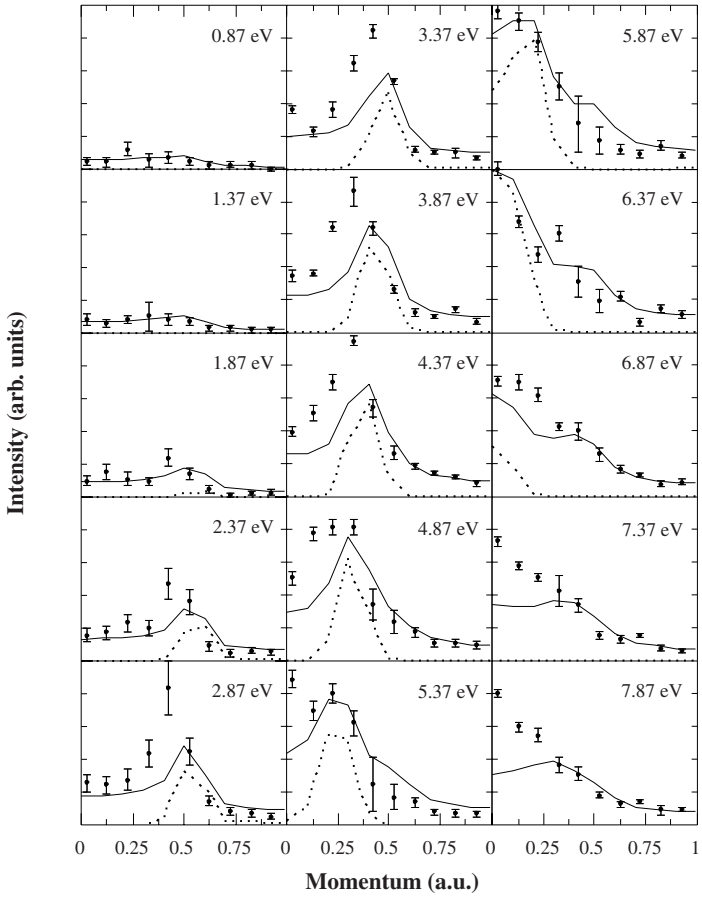

Figure 8. Momentum profiles for Ca integrated over 0.5 eV energy intervals from the experiment (points with error bars), the Monte Carlo (MC) simulation (solid lines) and the LMTO calculation (dashed lines). The three data sets have been normalized in the 6.37 eV momentum profile. The LMTO and MC curves have been shifted by 2.4 eV to match the experimental binding energy referenced to the vacuum level.

peaks, together with an additional Gaussian and second order polynomial in the case of experiment and MC simulation to account for the background under the peaks. A plot of the peak positions as a function of energy and momentum, i.e. the dispersion curve, for the experimental, LMTO and MC data are shown in figure 9. Dispersion curves have also been extracted from the momentum profiles of figure 8 by fitting a Gaussian to the peak and a fourth order polynomial to the background in the experimental and MC data. The results are also plotted in figure 9. The binding energy at the bottom of the band for all data sets has been set equal to 3.96 eV, which means that zero energy now corresponds to the Fermi level from the LMTO calculation.

Considering first dispersion curves extracted from the binding energy spectra, the theory and MC simulation follow each other reasonably well, albeit with a systematic shift downward of the MC curve relative to theory. The experimental dispersion points deviate from both theory and MC simulation, showing a maximum deviation of 1.2 eV at a momentum of 0.3 au. After reaching a maximum at 0.5 au the experimental points flatten off as do both the LMTO and MC

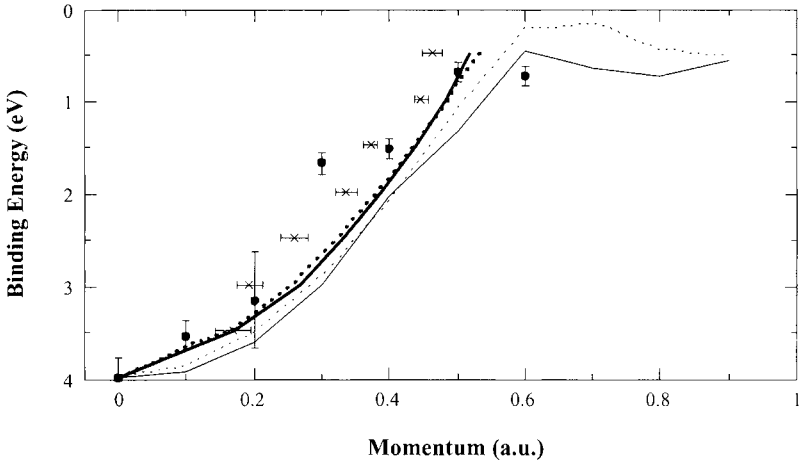

Figure 9. Conduction band dispersions for Ca derived from the experimental and theoretical data. Points with vertical error bars, thin solid line and thin dashed line are from the experimental, MC and LMTO binding energy curves respectively. Points with horizontal error bars, thick solid line and thick dashed line are from the experimental, MC and LMTO momentum profiles respectively. Energies at the bottom of the conduction band have been set equal to the LMTO value.

Table 2. Occupied conduction bandwidth in metallic calcium in eV.

Expt	LMTO + Monte Carlo	LMTO	Ref.
3.3 ± 0.2	3.51 ± 0.02	3.83 ± 0.01	Present
3.0 ± 0.2			[15]
6.8			[16]
3.6 ± 0.2			[14]
~ 7			[38]

curves. This flattening in the conduction band dispersion is an indication of the contribution of d states: bands derived from these states are expected to be significantly less dispersive than s-derived bands. Occupied conduction bandwidths can be obtained from these curves and are presented in table 2. The measured bandwidth agrees with the LMTO calculation to within the error when the MC simulation of the background is included in the theory.

Our measured bandwidths compare well with previous values of 3.0 ± 0.2 eV and 3.6 ± 0.2 eV obtained by Kingston [15] and Ley *et al* [14]. However, Skinner *et al* [38] and Finkelshteyn and Nemnona [16] report significantly higher values of around 7 eV, although the latter result could be affected by surface contamination.

The theoretical and MC dispersion curves derived from the momentum profiles agree very closely, but are both systematically wider in momentum by approximately 0.05 au compared with the experimental points. These curves do not appear to flatten off in energy near the top of the band; the peak intensity at this point is relatively small and is smeared along the momentum axis, making it difficult to reliably determine peak positions. Overall, there is good agreement between the dispersion curves obtained from the two methods described above up to a momentum value of 0.5 au.

The densities of occupied states (DOS) calculated from the experimental, LMTO and MC data by integrating the peak intensity in the corresponding momentum profiles over momentum

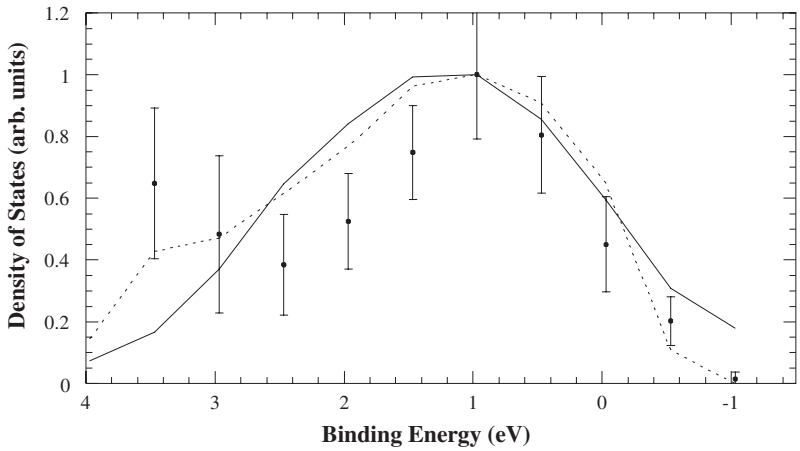

Figure 10. Density of occupied states for the conduction band of Ca extracted from the momentum profiles. Points with error bars are the experimental data, the solid curve is the Monte Carlo simulation and the dashed curve is the LMTO calculation. Binding energy is relative to the Fermi level.

space are shown in figure 10. In the integration the intensity is weighted with a phase space factor of the square of the electron momentum, q^2. Binding energies are relative to the Fermi level from the LMTO calculation. The DOS derived from the theoretical data does not fall sharply to zero at the Fermi level, as would be expected, because the LMTO calculation has been convoluted with Gaussians. For the same reason the LMTO derived DOS does not give zero density at the bottom of the band. Overall, the LMTO and Monte Carlo curves agree well, with the only differences occurring near the bottom and top of the band. Despite the large error bars, the experimental DOS shows a systematically smaller density in the middle of the band compared with both the calculated curves. This behaviour is consistent with the observation above that the dispersion curve is narrower in momentum for experiment compared with calculation. At a given binding energy the experimental intensity peaks at a smaller momentum value compared with theory and hence gives a smaller DOS value due to the phase space factor in the integral.

4.2. 3s and 3p core levels

From the same EMS experiment on calcium we have also measured the 3s and 3p core levels. These levels lie sufficiently close in energy that they can both be measured together with the conduction band in a single experimental run. The binding energy spectrum showing these two core levels and the conduction band is presented in figure 11. Binding energies are relative to the vacuum level, and the spectrum is integrated over a 2 au momentum range. The limited statistics in the core level peaks do not allow us to analyse the data in small momentum intervals and so we cannot determine the dispersion. In any case, dispersion of the core levels is expected to be small. The slightly asymmetric peak at about 28 eV corresponds to the Ca 3p core level and a broader feature at around 48 eV to the Ca 3s core level.

Core level binding energies have been determined by a least squares fit to the data in figure 11. The peaks themselves were fitted with Gaussians with three free parameters. In the case of the 3s level for which the intensity is concentrated around zero momentum, the intensity was integrated up to 1 au and the background under the peak approximated by a

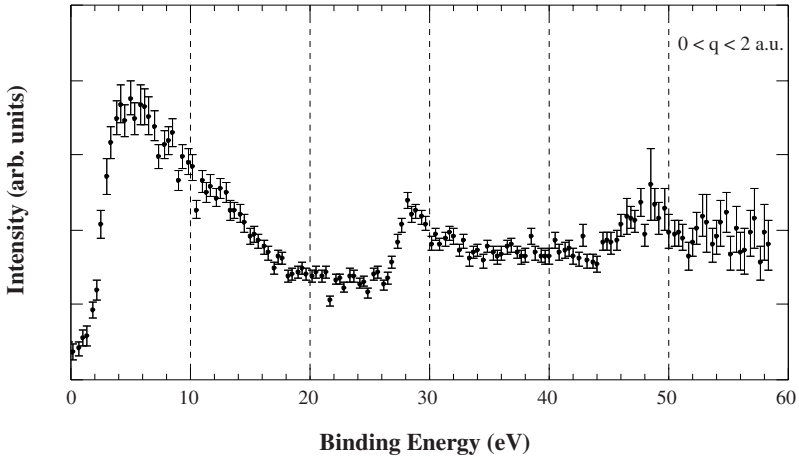

Figure 11. Binding energy spectrum integrated over a 2 au momentum range as measured by EMS showing the conduction band and two outermost core levels (3p and 3s) in metallic Ca. The energy is referenced to the vacuum level.

Table 3. Ca 3s and 3p core level positions in metallic Ca in eV. Energy is relative to the Fermi level.

3s	3p	Ref.
45.0 ± 0.4	25.6 ± 0.2	Present
44.1 ± 0.2	25.4 ± 0.2	[10]
44	26	[40]

straight line. For the 3p level integration was performed from 0.5 to 2 au momentum to get most of the signal, and the background was fitted by a second order polynomial. A summary of our data and those of two previous works for the core level positions is presented in table 3. Energies are referenced to the Fermi level with our values calculated using the experimental work function of 2.87 ± 0.2 eV measured by Gaudart and Rivoira [39] for polycrystalline calcium. For the 3s level our value differs from the XPS result obtained by Van Doveren and Verhoeven [10] by slightly more than the quoted errors, but for the 3p level both sets of data agree well. Siegbahn *et al* [40] obtained similar results.

5. Conclusion

We have measured the full energy and momentum resolved electronic structure of the conduction band, and the 3s and 3p core-level binding energies of calcium using electron momentum spectroscopy. We have also compared the experimental results to band structures calculated within the linear muffin-tin orbital approximation. An existing Monte Carlo simulation used to include multiple scattering effects in the calculated band structures has been updated. Band dispersions have been extracted from the experimental and theoretical data.

As expected, the dispersion curve resembles a free-electron-like parabola characteristic of a metallic solid. The results of the calculation plus simulation reproduce the experimental binding energy peaks and background intensities very well. This is in contrast to previous EMS results where the simulated background is at least 50% smaller than the experiment. Band

dispersions extracted from the experimental and calculated results behave slightly differently in the sense that the experimental curve has a narrower spread in momentum compared with theory. The occupied conduction bandwidth is slightly smaller in the experiment, but the difference from the Monte Carlo value is within the experimental error. The Ca 3s and 3p core level binding energies obtained in the experiment are in good agreement with those from previous measurements.

Acknowledgments

This work was supported by grants from the Australian Research Council and Flinders University. One of the authors (MAB) received support from the Shahid Bahonar University, Kerman, Iran, which allowed him to participate in this experiment. The authors acknowledge Professor I E McCarthy for providing the scattering cross-sections used in the Monte Carlo procedure.

References

[1] Mackintosh A R and Andersen O K 1980 *Electrons at the Fermi Level* (Cambridge: Cambridge University Press)
[2] Jan J P and Skriver H L 1981 *J. Phys. F: Met. Phys.* **11** 805
[3] Bakanov A A and Dudoladov I P 1967 *JETP Lett.* **5** 265
Balchan A S and Drickamer H G 1961 *Rev. Sci. Instrum.* **32** 308
Stager R A and Drickamer H G 1963 *Phys. Rev.* **131** 2524
Vereshchagin L F, Semerchan A A and Kuzin N N 1969 *Sov. Phys.–Dokl.* **14** 557
[4] Brennaa T D and Burdett J K 1993 *Inorg. Chem.* **32** 746
[5] Manning M F and Krutter L 1937 *Phys. Rev.* **51** 761
[6] Altmann S L, Harford A R and Blake R G 1971 *J. Phys. F: Met. Phys.* **1** 791
[7] Philips J C and Kleinmann L 1959 *Phys. Rev.* **116** 287
[8] Herring C 1940 *Phys. Rev.* **57** 1169
[9] Hohenberg P and Kohn W 1964 *Phys. Rev.* B **136** 864
Kohn W and Sham L J 1965 *Phys. Rev.* A **140** 1133
[10] Van Doveren H and Verhoeven J A T 1980 *J. Electron Spectrosc. Relat. Phenom.* **21** 265
[11] Leiro J A and Minni E E 1985 *Phys. Rev.* B **31** 8248
[12] Vayrynen J, Rantala T T, Minni E and Suoninen E 1983 *J. Electron Spectrosc. Relat. Phenom.* **31** 293
[13] Barth J, Chorkendorff I, Gerken F, Kunz C, Nyholm R, Schmidt-May J and Wendin G 1984 *Phys. Rev.* B **30** 6251
Barth J A, Gerken F and Kunz C 1983 *Phys. Rev.* B **28** 3608
[14] Ley L, Kerker G P and Martensson N 1981 *Phys. Rev.* B **23** 2710
[15] Kingston R H 1951 *Phys. Rev.* **84** 944
[16] Finkelshteyn L D and Nemnonov S A 1969 *Phys. Met. Metallorg.* **38** 38
[17] Coplan M A, Moore J H and Doering J P 1994 *Rev. Mod. Phys.* **66** 985
McCarthy I E and Weigold E 1991 *Rep. Prog. Phys.* **54** 789
[18] Dennison J R and Ritter A L 1996 *J. Electron Spectrosc. Relat. Phenom.* **77** 99
Fang Z, Guo X, Canney S A, Utteridge S, Ford M J, McCarthy I E, Kheifets A S, Vos M and Weigold E 1998 *Phys. Rev.* B **57** 4349
Vos M and McCarthy I E 1995 *J. Electron Spectrosc. Relat. Phenom.* **74** 15
[19] Canney S A, Vos M, Kheifets A S, Clisby N, McCarthy I E and Weigold E 1997 *J. Phys.: Condens. Matter* **9** 1931
[20] Canney S A, Sashin V A, Ford M J and Kheifets A S 1999 *J. Phys.: Condens. Matter* **11** 7507
[21] Sashin V A, Canney S A, Ford M J, Bolorizadeh M, Oliver D R and Kheifets A S 2000 *J. Phys.: Condens. Matter* **12** 125
[22] Canney S A, Brunger M J, McCarthy I E, Storer P J, Utteridge S, Vos M and Weigold E 1997 *J. Electron Spectrosc. Relat. Phenom.* **83** 65
Storer P, Caprari R S, Clark S A C, Vos M and Weigold E 1994 *Rev. Sci. Instrum.* **65** 2214
[23] McCarthy I E and Weigold E 1988 *Rep. Prog. Phys.* **51** 229

[24] Inokuti M 1971 *Rev. Mod. Phys.* **43** 297
[25] Utteridge S J, Sashin V A, Canney S A, Ford M J, Fang Z, Oliver D R, Vos M and Weigold E 2000 *Appl. Surf. Sci.* **162/163** 357
[26] Egerton R F 1996 *Electron Energy-Loss Spectroscopy in the Electron Microscope* (New York: Plenum)
[27] Leder L B and Suddeth J A 1960 *J. Appl. Phys.* **31** 1422
[28] Quinn J J 1962 *Phys. Rev.* **126** 1453
[29] Kheifets A S, Lun D R and Savrasov S Y 1999 *J. Phys.: Condens. Matter* **11** 6779
[30] Wyckoff R 1963 *Crystal Structures* (New York: Interscience)
[31] Gaspar R 1954 *Acta Phys. Acad. Sci. Hung.* **3** 363
[32] Kheifets A S and Vos M 1995 *J. Phys.: Condens. Matter* **7** 3895
[33] Vos M and Bottema M 1996 *Phys. Rev.* B **54** 5946
[34] Guo X, Fang Z, Kheifets A S, Canney S A, Vos M, McCarthy I E and Weigold E 1998 *Phys. Rev.* B **57** 6333
[35] Robins J L and Best P E 1962 *Proc. Phys. Soc.* **79** 110
[36] Langkowski J 1975 *J. Phys. D: Appl. Phys.* **8** 2058
[37] Lundqvist B I 1969 *Phys. Status Solidi* **32** 273
[38] Skinner H W B, Bullen T G and Johnston J E 1954 *Phil. Mag.* **45** 1070
[39] Gaudart L and Rivoira R 1971 *Appl. Opt.* **10** 2336
[40] Siegbahn K *et al* 1967 *ESCA, Nova Acta Regiae Soc. Sci. Ups.* Ser. IV, 20